Journal of ELECTRONIC MATERIALS, Vol. 48, No. 7, 2019
https://doi.org/10.1007/s11664-019-07229-z

Facile Synthesis of 4-Methylaniline Reduced Graphene Oxide/Polyaniline Composite for Supercapacitors

NALI CHEN,[1,2,3] CHIHUAN LIU,[2] LIN TAN,[2] YAPENG REN,[2] DAN ZHAO,[2] YONGCHUN LUO,[1,4] and HUIXIA FENG[2,5]

1.—School of Materials Science and Engineering, Lanzhou University of Technology, Lanzhou 730050, Gansu, People's Republic of China. 2.—College of Petrochemical Technology, Lanzhou University of Technology, Lanzhou 730050, Gansu, People's Republic of China. 3.—e-mail: chennl2007@126.com. 4.—e-mail: luoyc@lut.cn. 5.—e-mail: fenghx@lut.cn

A promising material for supercapacitors based on 4-methylaniline reduced graphene oxide/polyaniline (GP) composite was successfully prepared through a facile one-pot synthesis route. During the preparation process, 4-methylaniline acted as a reducing agent for graphene oxide (GO) as well as a spacer for the resulting reduced graphene oxide (RGO) sheets. The characterization results reveal that GO was successfully reduced by 4-methylaniline and the RGO sheets covered by polyaniline (PANI) nanowires retain favorable dispersibility in the GP composite. The GP composite shows a high specific capacitance (530.4 F g^{-1} at 0.5 A g^{-1}) with a good cycling stability (87.61% retention after 3000 cycles). Moreover, the GP composite also delivers a good rate performance of 77.5% retention from 0.5 A g^{-1} to 20 A g^{-1}, but for the graphene oxide/polyaniline (GOP) composite and pure PANI, the retentions are only 47.2% and 28.9%, respectively.

Key words: Supercapacitors, polyaniline, 4-methylaniline, reduced graphene oxide, rate performance

INTRODUCTION

Supercapacitors, known as electrochemical capacitors, have received tremendous attention in a wide range of applications as energy storage devices because of their high power density, long cycle life, small environmental impact, high margin of safety, and low maintenance.[1,2] Their performance mainly depends on the electrode material and electrolyte. Polyaniline (PANI) is a promising electrode material for supercapacitors because of its facile synthesis, low preparation cost, environmental stability, and high redox pseudocapacitive storage.[3,4] However, the practical application of a PANI electrode in supercapacitors is seriously limited due to the low rate performance and poor cycling stability. To combat these problems, nano-sized PANIs with various morphologies[5,6] and a large number of PANI-based composites have been explored.[7–14] The composites composed of carbonaceous material (such as carbon spheres,[7] carbon nanotubes,[8,9] mesoporous carbon,[10] N-doped porous carbon,[11] carbon black,[12] graphene,[13,14]) and PANI, especially graphene/polyaniline composites, have been extensively studied as the electrode materials for supercapacitors due to their outstanding electrochemical performances as a result of the combination of advantages of each component and their synergistic effects. Graphene/polyaniline composites, which combine the high specific capacitance of PANI and the good cycling stability, excellent electrical conductivity and large specific surface area[15] of graphene, achieve excellent electrochemical performance.

Because of the strong π–π interactions, graphene sheets tend to re-stack, which influences the nanostructure of graphene/polyaniline composites and their energy storage ability. Therefore, the

(Received August 9, 2018; accepted April 16, 2019; published online April 24, 2019)

dispersibility of the graphene sheets is a vital problem that must be considered during the preparation process of graphene/polyaniline composites. Many methods have been developed to improve the dispersibility of the graphene sheets in the composites. Some researchers prepared the graphene/polyaniline composites by the polymerization of aniline in the presence of graphene oxide (GO) or GO hydrogel followed by reduction[16–18]; Hasan et al.[19] reported the synthesis of graphene/polyaniline composites by the *in situ* polymerization of aniline in graphene dispersion containing surfactant; Cai et al.[20] reported the preparation of graphene/polyaniline composites through the physical mixing of graphene and PANI with the assistance of surfactant; Zhao et al.[21] developed a strategy to prepare graphene/polyaniline composites, which included the preparation of graphene hydrogels followed by the i*n situ* polymerization of aniline. Jin et al.[22,23] and our group recently synthesized graphene/polyaniline composites through a one-pot method with aniline as reductant for GO and the monomer of subsequent *in situ* polymerization. During the reduction process, aniline could convert GO into graphene [sometimes called reduced graphene oxide (RGO)] and simultaneously oxidized itself to aniline oligomers. These aniline oligomers were adsorbed on the surface of the resulting graphene sheets through π–π interaction, and thus ensured the good dispersibility of graphene sheets in the composites. 4-methylaniline, which contains a weak electron-donating substituent group compared to aniline, can more easily convert GO into RGO and, therefore, has a higher efficiency of reduction. Furthermore, 4-methylaniline is also a spacer, which prevents aggregating and re-stacking of the graphene sheets due to the presence of a π–π interaction between 4-methylaniline or its oxidation product and RGO sheets.

In the present work, an effective one-pot synthesis method for the preparation of reduced graphene oxide/polyaniline (GP) composite is reported. The RGO dispersion was prepared by reducing GO with 4-methylaniline as a reductant, which only took 1 h in a 95°C water bath. Subsequently, the GP composite was prepared by the chemical oxidative polymerization of aniline in the resulting RGO dispersion. The results of structure characterization shows the GO was successfully reduced by 4-methylaniline and the RGO sheets covered by PANI nanowires remains well-dispersed in the GP composite. Moreover, the GP composite delivers an outstanding rate capability of 77.5% retention from 0.5 A g^{-1} to 20 A g^{-1}, showing a high specific capacitance (530.4 F g^{-1} at 0.5 A g^{-1}) and an excellent cycling stability (87.61% retention after 3000 cycles at 100 mV s^{-1}). So 4-methylaniline is an appropriate reducing agent for GO and a spacer for the resulting RGO sheets, and the GP composite may have potential application as electrode material for supercapacitors.

EXPERIMENTAL SECTION

Materials

Graphite powder (325 mesh, Kaitong Co., LtD., Tianjin, China), 4-methylaniline (Institute of Chemical Physics, Chengdu, China). Aniline monomer was distilled under pressure before use. Other chemicals were analytical grade without further purification.

Preparation of RGO Dispersion

GO was synthesized from commercially available graphite powder by a modified Hummer's method, which is mentioned in previous work in detail.[24] Ten milligrams of GO was dispersed in deionized water followed by sonicating, and a brown dispersion was obtained. Fifty milligrams of 4-methylaniline was added into the above dispersion and sonicated. Then the obtained mixture was transferred into a water bath at 95°C for 1 h under magnetic stirring, during which GO was reduced by 4-methylaniline. A black dispersion of RGO was obtained.

Preparation of GP Composite

The GP composite was prepared by the low-temperature chemical oxidative polymerization of aniline in the dispersion of RGO, following a method reported previously.[25] In the procedure, 0.33 mL aniline was added into the RGO dispersion containing hydrochloric acid. The obtaining mixture was sonicated for several minutes, then transferred to the ice bath. Afterwards, ammonium persulfate (APS) (molar ratio: APS/aniline = 1:1) was dissolved in 10 mL deionized water then cooled to 0°C and dropwise added into the above mixture with vigorous stirring. The color of the solution changed from black to dark green. After 24 h, the product was collected by filtering, washed with water and ethanol. Finally, the product dried in a vacuum oven at 80°C for 12 h.

For comparison, pure PANI and graphene oxide/polyaniline (GOP) composite were prepared through a same process only using deionized water and exfoliated GO dispersion instead of RGO dispersion, respectively.

Structure Characterizations

Fourier transform infrared spectroscopy (FTIR, JRT-7000; JASCO, Japan) was used to analyze the molecular structure of products. The crystallographic structure was analyzed x-ray diffraction (XRD). The XRD patterns of the samples were collected using an XRD-6000 (Shimadzu Co., Ltd. Kyoto, Japan) with Cu Kα radiation scanning from 5° to 60°. Raman spectra were collected on a Renishaw 1000 confocal Raman microprobe (Renishaw instruments) with the 514 nm argon ion laser used for excitation. UV–Vis absorption spectra of the samples were taken in a quartz cells with light

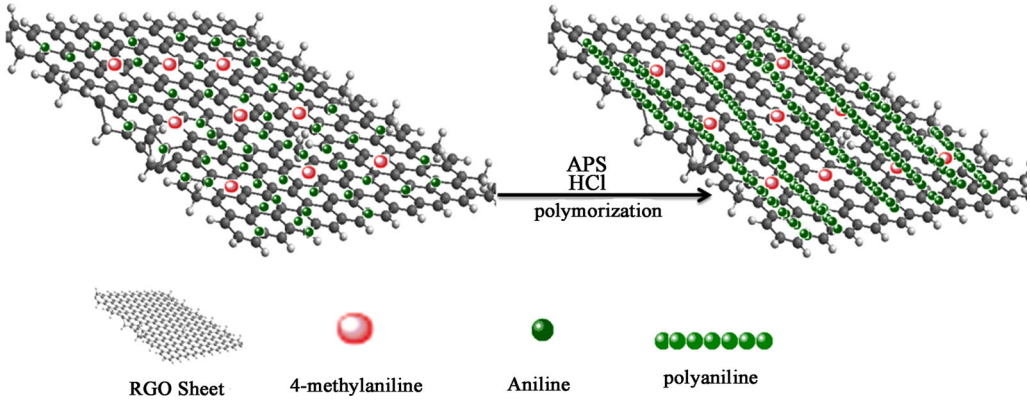

Fig. 1. Illustration of the process for the preparation of GP composite.

path of 1 cm on a TU-1810 UV–Vis spectrophotometer (Beijing Purkinje General Instrument, China). The microstructures of the products were surveyed by transition electron microscopy (TEM, H-8110, Hitachi Co., Ltd. Tokyo, Japan) and scanning electron microscopy (SEM, S-4300, Hitachi Co., Ltd. Tokyo, Japan). The specific surface areas and pore distribution of the samples were measured using a Micromeritics ASAP 2020 volumetric adsorption analyzer at 77 K.

Electrochemical Tests

All electrochemical properties of the samples were explored with a three-electrode system on a CHI 660E electrochemical workstation in 1 M H_2SO_4 aqueous electrolyte solution. By mixing 80 wt.% active material with 10 wt.% acetylene black and 10 wt.% polytetrafluoroethylene dispersed in ethanol we obtained a slurry. The slurry was coated and pressed on a 1×1 cm^2 stainless steel mesh, which was used as the working electrode. The mass of the active material loading of the working electrode was typically 4 mg cm^{-2} after dried in vacuum at 80°C for 12 h. The platinum wire and saturated calomel electrode (SCE) were used as the counter and reference electrodes, respectively. Cyclic voltammetry (CV) tests were carried out at various scan rates from 5 mV s^{-1} to 50 mV s^{-1}. Galvanostatic charge/discharge (GCD) tests were performed at various current densities from 0.5 to 20 A g^{-1}. The voltage range for the CV and GCD tests was from − 0.2 V to 0.7 V. Electrochemical impedance spectroscopy (EIS) tests were performed in a frequency range from 0.01 Hz to 100 kHz at 5 mV amplitude to open circuit potential.

RESULTS AND DISCUSSION

Formation Process of GP Composite

Aniline is applied as a reducing agent for GO to prepare the GP composite with a good electrochemical performance.[22,23] 4-methylaniline possesses a stronger reducing action than aniline. In this work, 4-methylaniline was employed as a reducing agent to prepare RGO, followed by the *in situ* chemical oxidative polymerization of aniline to prepare GP composite. 4-methylaniline reacted with the oxygen-containing functional groups on the surface of GO sheets to form the RGO dispersion. During the reaction process, 4-methylaniline released electrons and GO was converted into RGO by accepting the released electrons. The 4-methylaniline and its oxidized product were absorbed on the surface of the RGO sheets owing to the π–π interaction. Thus, the restacking of the RGO sheets was inhibited. After hydrochloric acid and aniline monomers were successively added into the resulting RGO dispersion, aniline monomers could immediately be adsorbed on the surface of resulting RGO sheets due to the stronger electrostatic attraction.[26] Then, as APS aqueous solution was dropwise added into the above mixture, the aniline underwent a polymerization just from the adsorbed sites on the surface of RGO sheets, and thus the PANI-coated RGO sheet gradually formed. This morphology, which is formed by the interaction of RGO sheets with PANI, promotes ion diffusion and electron transfer, producing a synergistic effect on the electrochemical properties of the composite. The formation process of GP composite is shown in Fig. 1.

Microstructure Characterization

Figure 2 shows the FT-IR spectra of the GO, RGO, pure PANI, GOP and GP composites. For GO, the characteristic peaks appear at 3420 cm^{-1}, 1735 cm^{-1}, 1625 cm^{-1}, 1412 cm^{-1} and 1070 cm^{-1}, indicating the presence of oxygen-containing functional groups on the surface of GO sheets. The absorption peaks at 3420 cm^{-1}, 1735 cm^{-1} and 1412 cm^{-1} are assigned to the stretching vibration of the O–H, C=O, and C–OH from the COOH groups, respectively. The peak at 1070 cm^{-1} is attributed to the stretching vibration of C–O.[20,27,28] The absorption peak about at 1625 cm^{-1} is attributed to the stretching vibration of C=C. In contrast, for RGO, the intensities of the all peaks correlated to the oxygen-containing functional

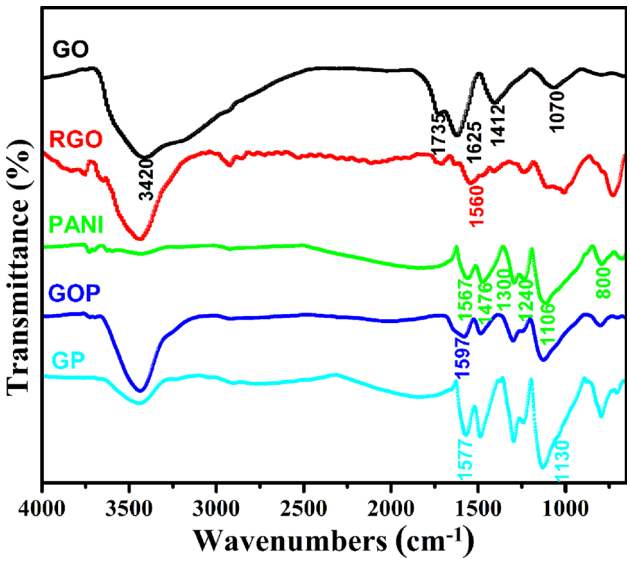

Fig. 2. FT-IR spectra of GO, RGO, PANI, GOP and GP composites.

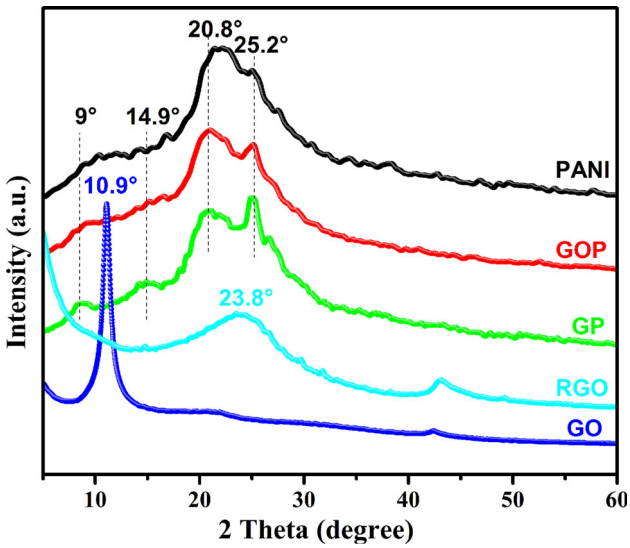

Fig. 3. XRD patterns of GO, RGO, PANI, GOP and GP composites.

groups are dramatically weakened. Furthermore, the peak at 1625 cm^{-1} attributed to C=C vibration is shifted to 1560 cm^{-1} in the spectrum of RGO, showing the recovery of the sp^2 hybrid carbon skeleton.[29] This confirms that GO was successfully reduced by 4-methylaniline. For the pure PANI, the vibration peaks are observed at 1567 cm^{-1}, 1476 cm^{-1}, 1300 cm^{-1}, 1240 cm^{-1}, 1106 cm^{-1} and 800 cm^{-1}. The peaks at 1567 cm^{-1} and 1476 cm^{-1} are attributed to C=C stretching deformations of the quinoid and benzenoid rings, respectively. The peaks at 1300 cm^{-1} and 1240 cm^{-1} are related to C–N and C=N stretching vibrations, respectively. In addition, the peaks at 1106 cm^{-1} and 800 cm^{-1} are assigned to the in-plane bending and out-of-plane bending vibrations of C–H, respectively.[25,30] The spectra of the GOP and GP composites elucidate the characteristic peaks of both GO or RGO substrate and PANI. For the GP composite, the peak at 1567 cm^{-1} associated with the quinoid rings shifted to 1577 cm^{-1}, which is possible because of the withdrawing induction effect of C=O groups from RGO. The shift is more obvious (from 1567 cm^{-1} to 1597 cm^{-1}) in the spectrum of the GOP composite. These observations corroborate the formation of GP and GOP composites. Moreover, for the GP composite, the peak at 1130 cm^{-1} related to the PANI conductivity was enhanced,[31] which is attributed to π–π interaction between the conjugated PANI chains and RGO sheets. The π–π interaction might effectively transfer the faradic reaction charges from the PANI to the RGO sheets,[32] which will benefit the electrochemical properties of the GP composite.

Figure 3 illustrates the XRD patterns of the GO, RGO, pure PANI, GOP and GP composites. The GO shows a sharp intense diffraction peak at 2θ = 10.9°, which corresponds to a large d-spacing of 0.82 nm, indicating full oxidation.[33] After reduction, the peak at 10.9° disappears while a new broad reflection peak centered at 2θ = 23.8° appears. The d-spacing value of the RGO decreases to 0.37 nm, slightly higher than that of natural graphite.[34] This demonstrates that there are still some residues left on the surface of graphene sheets. This change in the d-spacing value can be attributed to the almost complete reduction of GO and formation of graphitic structures. For the XRD patterns of the pure PANI, GOP and GP composites, the almost same peaks (at about 14.9°, 20.8° and 25.2°) corresponding to (011), (020) and (200) planes of PANI are observed, indicating the presence of the same crystal type of PANI in the pure PANI, GOP and GP composites.[35] Meanwhile, the intensity of diffraction peaks of the GOP and GP composites is increased in comparison with the pure PANI, suggesting that a higher crystallinity degree of PANI in composites, particularly in the GP composite. This is possible due to the PANI was grown on the surface of RGO sheets, which confined spaces can guide the orientation of PANI chains[36,37] and result in a high crystallinity. However, the typical peaks of the GO and RGO completely disappear in the GOP and GP composites, respectively, which may be covered by the diffraction peaks of the PANI.

Raman spectroscopy is widely used to characterize the structural changes and electronic properties of graphene-based materials. Figure 4 shows the Raman spectra of the GO, RGO, pure PANI, GOP and GP composites. The spectra of both GO and RGO display two prominent bands at about 1351 cm^{-1} assigned to the D-band and at about 1596 cm^{-1} assigned to the G-band. The D-band represents the conversion of carbon from sp^2-hybridized to sp^3-hybridized while the G-band corresponds to the in-plane bond stretching motion of C-sp^2 atoms.[38] The change in the relative intensity of the D and G-band (D/G) indicates the change of the

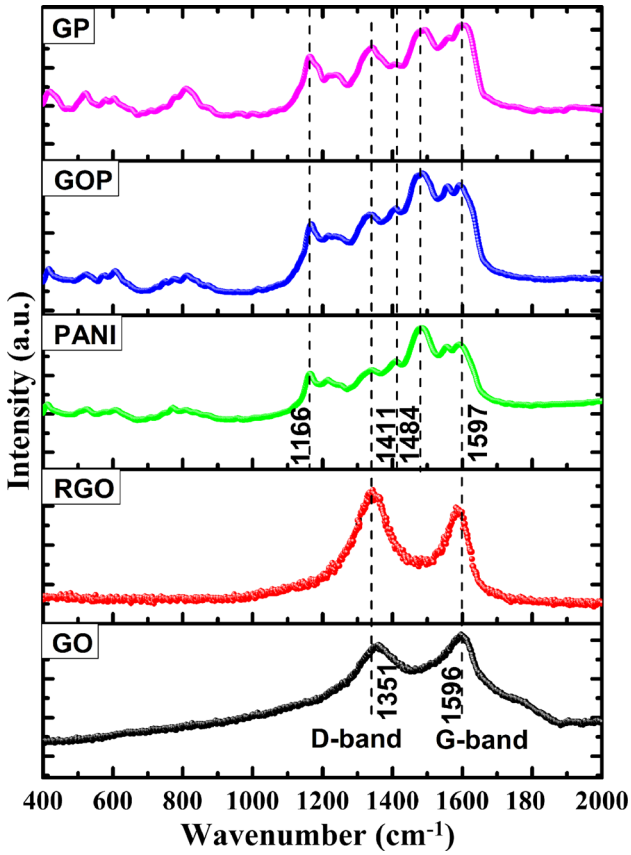

Fig. 4. Raman spectra of GO, RGO, PANI, GOP and GP composites.

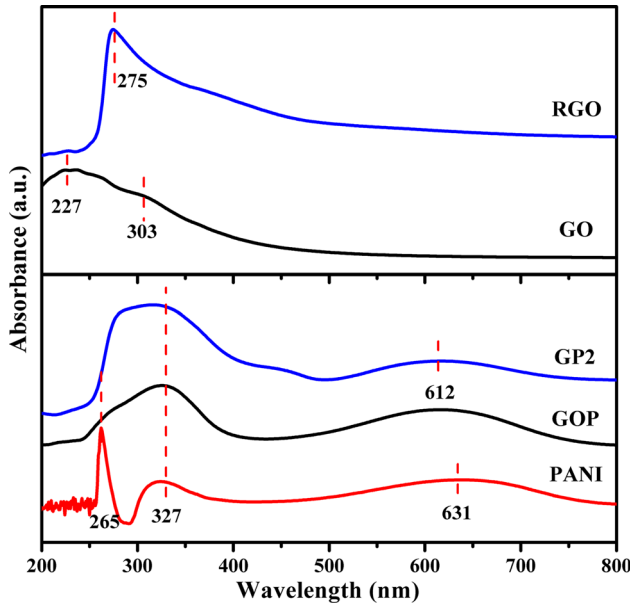

Fig. 5. Uv-vis patterns of GO, RGO, pure PANI, GOP and GP composites.

electronic conjugation state of GO during the reduction process.[39] Meanwhile, the D/G intensity ratio of RGO (1.21) is increased in comparison with that of GO (0.93), suggesting that numerous in-plane sp^2 domains of conjugated carbon atoms formed during the reduction process of the GO. For the pure PANI, the characteristic peaks appear at 1166 cm^{-1}, 1411 cm^{-1}, 1484 cm^{-1} and 1597 cm^{-1}, corresponding to C–H bending vibration of the quinoid ring, C–C stretching vibration of quinoid rings, C=N stretching vibration of quinoid rings, and C–C stretching vibration of benzenoid,[40] respectively. The spectra of the GOP and GP composites are similar to that of the PANI, which is attributed to the growth of PANI on the surface of the GO and RGO sheets, respectively. Meanwhile, it can be observed that the intensities of bands at about 1350 cm^{-1} and 1590 cm^{-1} of the GOP and GP composites were increased in comparison with that of the PANI. Moreover, the intensity ratio of G/D bands of the GP composite increases compared with that of the GOP composite, which is attributed to the larger influence of the PANI nanowires on the RGO, which is consistent with the previous reports.[41]

Figure 5 shows the Uv–Vis patterns of the GO, RGO, pure PANI, GOP and GP composites. The spectrum of the GO presents a C=C plasmon peak at around 227 nm (π–π^* transition) and a shoulder band at 303 nm (n–π^* transitions of C=O).[42] Compared with GO, the shoulder band loses intensity and the plasmon peak at 227 nm is red-shifted to 275 nm in the Uv–Vis patterns of RGO, reflecting the increase of π-electron density and structural ordering resulting from the restoration of the sp^2 carbon and possible rearrangement of atoms. These observations also suggest the successful reduction of GO with 4-methylaniline.[43] The PANI has a strong π–π^* peak at 265 nm, a medium π–π^* peak at 327 nm, and a very weak n–π^* absorption at about 631 nm.[44] After the grown of PANI nanowires on the surface of the GO or RGO sheets, the gap at the low wavelength disappears and the peak at about 631 nm is still observed. Compared with the GOP composite, the GP composite shows a broader peak at the low wavelength. The results indicate that the electrons in the GP composite have been more delocalized[45] and the stronger π–π interaction between two components formed, which is beneficial to the improvement of the electrochemical performances of composite.

The SEM and TEM images of the prepared samples are shown in Figs. 6 and 7. The pure PANI exhibits worm-like nanorods that are dozens of nanometers in length and several of nanometers in width, randomly stacking to form agglomerates (see Figs. 6a and 7b). The extremely dense structure of PANI lacks the ordered passages, which seriously obstructs the transport directionally of electrolyte ions.[26] As shown in Fig. 7a, RGO displays a typically layered structure with wrinkles, and the inset in Fig. 7a is the selected area electron diffraction (SAED) pattern, which can reveal the crystal structure of the RGO obtained via the chemical reduction of the GO with 4-methylaniline. The diffraction

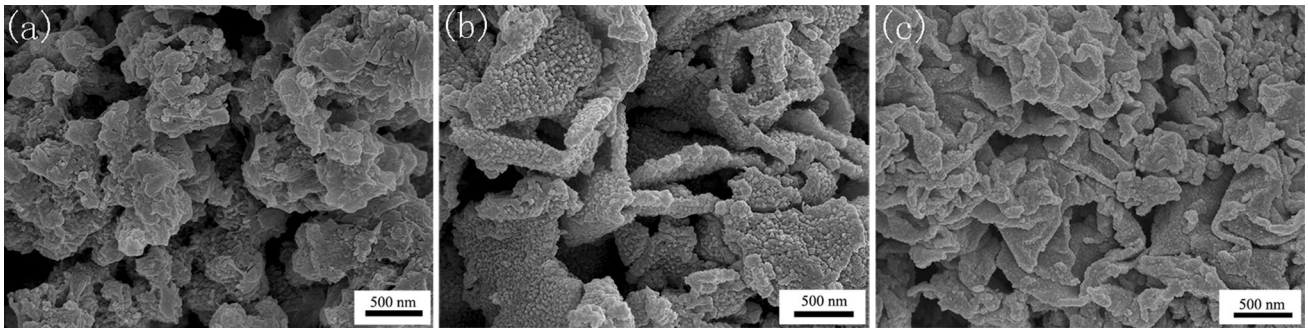

Fig. 6. SEM images of PANI (a), GOP (b), and GP (c) composites.

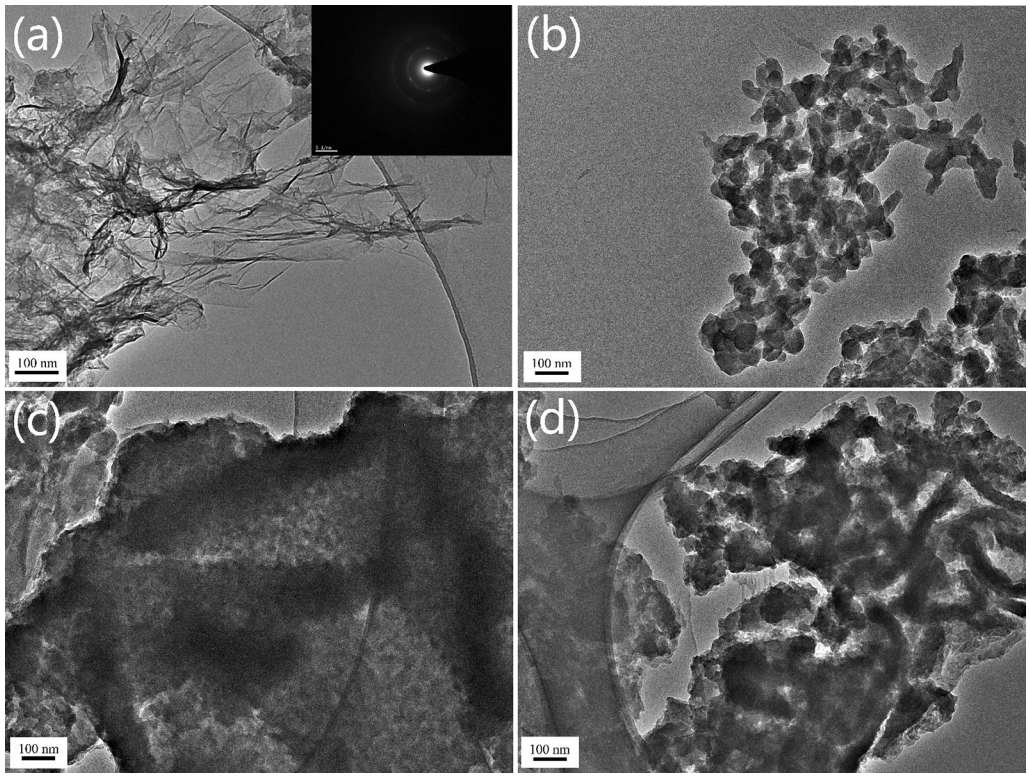

Fig. 7. TEM images of RGO (a), PANI (b), GOP (c) and GP (d) composites. The inset in (a) shows the SAED patterns of RGO.

rings indicate that the obtained RGO presents the turbostratic stacking, and the similar results have also been found in other work.[46] In comparison with the pure PANI, the GOP and GP composites show a significantly different morphology. Because of the substrate function of the GO and RGO sheets during the *in situ* polymerization process of aniline, the nanometer-sized PANIs are respectively dispersed on the surface of the GO and RGO sheets in GOP and GP composites, forming the PANI-covering layer-like structure with a large interfacial surface area (see Figs. 6b and c and 7c and d). This is one reason why the composites with the PANI-covering layer-like structure display better electrochemical performances than the randomly stacking pure PANI. The GP composite shows a curly layer-like structure as shown in Fig. 6c. Furthermore, in the GP composite, the PANI nanowires are coated on the surface of well-dispersed RGO sheets (see Figs. 6c and 7d) and two components are closely integrated together. These structural characteristics of the GP composite can reduce the diffusion path and diffusion resistance of electrolyte ions into the electrode matrix and also decrease the interfacial charge-transfer resistance between two components, improving the electrochemical performances of the GP composite.[47]

The microstructure of the GP composite was further characterized by nitrogen adsorption and desorption at 77 K as shown in Fig. 8. Based on the N_2 adsorption–desorption experiment, the BET surface area of GP composite is 40.61 $m^2\ g^{-1}$, which

is much higher than that of the pure PANI (17.59 m^2 g^{-1}) reported in the literature.[48] The higher BET surface area of the composite can be attributed to the homogeneous dispersion of PANI and RGO sheets. Moreover, The pore size distribution calculated by the BJH method in Fig. 8 (inset) clearly shows that the majority of the pore volume and surface area are from the mesopores and macropores.

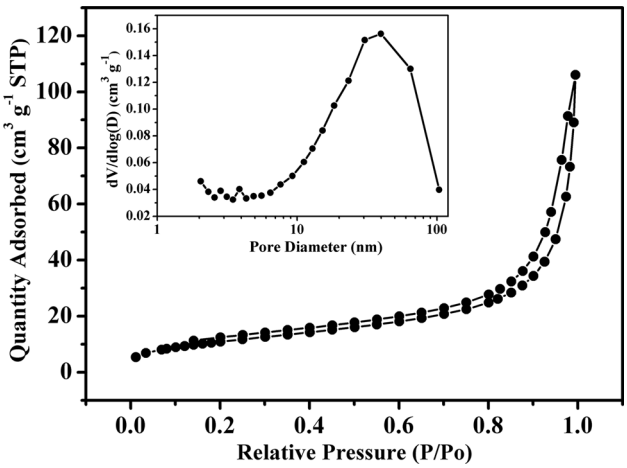

Fig. 8. Nitrogen adsorption/desorption isotherm and BJH pore size distribution (inset) of GP composite.

Electrochemical Performance

The electrochemical performance of the pure PANI, GOP and GP composites was characterized by CV, GCD, EIS and cycling stability tests using a conventional 3-electrode setup in 1.0 M H_2SO_4. Figure 9a shows the comparative CV curves of the pure PANI, GOP and GP composites at 5 mV s^{-1} in the potential range from − 0.2 V to 0.7 V. It can be seen that the CV curves of the three samples present the typical pseudocapacitance behavior of the PANI, which are attributed to the redox reaction. Specifically, the redox reaction are ascribed to the transition between leucoemeraldine/emeraldine and emeraldine/pernigraniline of PANI.[49] However, the enclosed area by the CV of the composites (GOP and GP) is larger than that of the pure PANI, which indicates that the composites possess a higher relative specific capacitance. More specifically, the GOP composite exhibits only a marginal improvement in specific capacitance from the pure PANI, while the GP composite has much more significant improvements.

Figure 9b shows the comparative GCD curves of the pure PANI, GOP and GP composites at 0.5 A g^{-1}. Humps appear on the discharge curves of the three samples, revealing that the faradic reactions happen in the process of discharging. From these curves, it is easy to get the specific capacitances (C_m in F g^{-1}) of the samples by the Eq. 1 as follows:

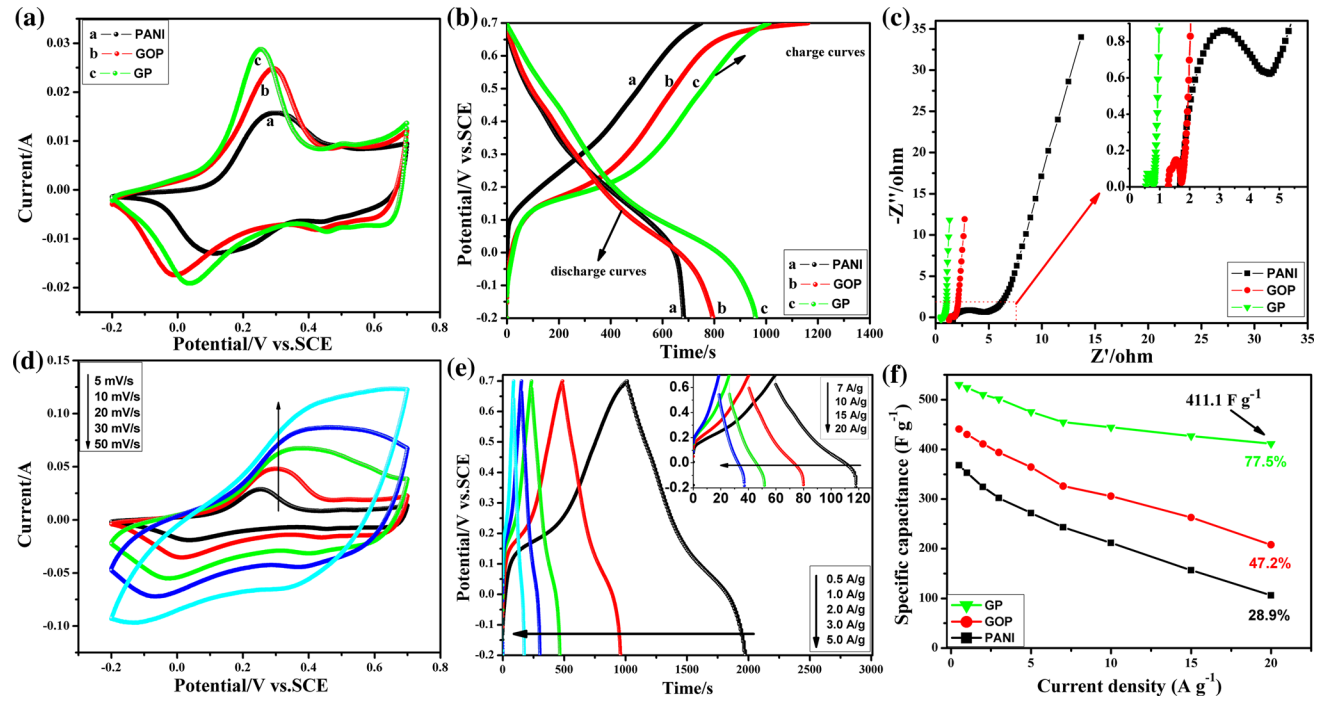

Fig. 9. Electrochemical characterization of PANI, GOP and GP composites. (a) CV, (b) GCD, (c) EIS, the inset showing the magnified high-frequency regions, (d) CV curves of the GP composite at various scan rates, (e) GCD curves of the GP composite at 0.5 A g^{-1}, 1 A g^{-1}, 2 A g^{-1}, 3 A g^{-1} and 5 A g^{-1}, the inset showing the GCD curves of the GP composite at 7 A g^{-1}, 10 A g^{-1}, 15 A g^{-1} and 20 A g^{-1} and (f) specific capacitance as a function of the current density.

Table I. The comparison of the capacitive performances of the reported graphene/PANI composites and the present work

Electrode materials	Specific capacitance (F g^{-1})		Rate performance	Cycling stability
Graphene/PANI aerogel[49]	520.3 (0.25 A g^{-1})	–	64% (0.25–2A g^{-1})	–
Three-dimensional graphene-PANI hollow sphere[50]	456 (0.5 A g^{-1})	290 (20 A g^{-1})	64% (0.5–20 A g^{-1})	83% (1000, 0.5 A g^{-1})
3D rGO aerogel/PANI array[51]	432 (1 A g^{-1})	352 (20 A g^{-1})	81.4% (1–20 A g^{-1})	–
Graphene/PANI hydrogel[52]	307 (0.2 A g^{-1})	–	48.9% (0.2–5 A g^{-1})	90% (1000, 1 A g^{-1})
PANI/graphene hydrogel[54]	610 (1 A g^{-1})	350 (20 A g^{-1})	57.4% (1–20 A g^{-1})	94.4% (1000, 20 A g^{-1})
This work	530 (0.5 A g^{-1})	411 (20 A g^{-1})	77.5% (0.5–20 A g^{-1})	87.61% (3000, 100 mv s^{-1})

$$C_m = \frac{I \times t}{\Delta V \times m} \quad (1)$$

where ΔV is the potential range (in V), m is the mass of the active material in the working electrode (in g), I and t are the current (in A) and time (in s) in the process of discharge respectively.[47] From the Eq. 1, the GP composite with the longest discharging time achieves the highest specific capacitance. The specific capacitances of the pure PANI, GOP and GP composites are 367.9 F g^{-1}, 440.9 F g^{-1} and 530.4 F g^{-1}, respectively. The GOP and GP composites present a higher specific capacitance than the pure PANI. The specific capacitance of the GOP composite only has a marginal improvement from pure PANI (e.g. 440.9 F g^{-1} versus 367.9 F g^{-1} at 0.5 A g^{-1}), while the specific capacitance of the GP composite has much more significant improvements from 367.9 F g^{-1} to 530.4 F g^{-1}. These results are in accordance with those deduced from the CV curves. Meanwhile, the specific capacitance of the GP composite is also higher than those of the recently reported graphene/polyaniline composites (see Table I), such as hierarchical graphene/PANI hybrid aerogels (520.3 F g^{-1}),[49] three-dimensional graphene-PANI hybrid hollow sphere (456 F g^{-1}),[50] three-dimensional RGO aerogel/PANI array (432 F g^{-1}),[51] and graphene/PANI composite hydrogel (307 F g^{-1}).[52] The enhanced specific capacitance of the composites (GOP and GP) originates from two components of composites and their synergistic effects. Moreover, the specific capacitance of the GP composite is higher compared with that of the GOP composite. This is attributed to the following: the conductivity of the RGO prepared by reducing GO with 4-methylaniline is higher, the interaction between the PANI nanowires and the RGO sheets is stronger, and the GP composite shows a curly layer-like structure.

The electrochemical impedance tests were carried out for the pure PANI, GOP and GP composites to further investigate the charge transfer kinetics and the ion diffusion rate. The results are shown in Fig. 9c. The internal resistance (R_s) of the GP composite is 0.52 Ω, lower than those of the GOP composite (1.27 Ω) and the pure PANI (1.66 Ω). The lower internal resistance wastes less energy during charging-discharging processes, which is important for energy storage devices. The interfacial charge-transfer resistance (R_{ct}) of the GP composite is 0.35 Ω, also lower than those of the GOP composite (0.64 Ω) and the pure PANI (3.25 Ω). The R_s and R_{ct} of the GP composite are the smallest, suggesting that the GO was successfully reduced by 4-methylaniline, indicating that the introduction of RGO enhances conductivity and improves the charge transfer performance of the composite electrode. In addition, the curve length in the Warburg region is related to the ion diffusion in the electrolyte/electrode interface.[53] The Warburg region of the GP composite is shorter than those of the GOP composite and the pure PANI, indicating the shorter ion diffusion path for the GP composite. This could promote the efficient access of the electrolyte ions to the GP electrode surface.

To get more information on the capacitive performances of the resulting composite, the GP electrode was selected for the measurement in detail. Figure 9d shows the CV curves of the GP composite in a wide range of scan rates (5–50 mV s^{-1}). It can be seen that the redox current of the GP composite clearly increases with the increasing scan rate and the redox peaks are still observed at a high scan rate (50 mV s^{-1}), indicating a good rate capability for the GP composite. Because of the resistance of the electrode, the oxidation and the reduction peaks shift positively and negatively, respectively, as the scanning rate increases. The GCD measurements of the GP composite in 1 M H_2SO_4 solution were carried out at 0.5 A g^{-1}, 1.0 A g^{-1}, 2.0 A g^{-1}, 3.0 A g^{-1}, 5.0 A g^{-1}, 7.0 A g^{-1}, 10 A g^{-1}, 15 A g^{-1} and 20 A g^{-1}. The curves at different current densities show a deviation from the ideal triangular shape (Fig. 9e), exhibiting a pseudocapacitive characteristic and demonstrating a sustainable behavior for the GP composite even at a high current density of 20 A g^{-1}. These results are consistent with those obtained from the CV curves at different scan rates. The specific capacitances of the pure PANI, GOP and GP composites at different current densities were calculated and shown in Fig. 9f. From Fig. 9f, the increase of the current density results in the

decrease of specific capacitance for the three samples and the GP composite shows the best electrochemical performance. Upon increasing the current density up to 1.0 A g^{-1} and 5.0 A g^{-1} from 0.5 A g^{-1}, the GP composite delivers the specific capacitance of 524 F g^{-1} and 475.6 F g^{-1}, corresponding to the specific capacitance retention of 98.8% and 89.7%, respectively. Even at a high current density of 20 A g^{-1}, the specific capacitance still remains at 411.1 F g^{-1}, which is higher than the recently reported values of 290 F g^{-1},[50] 350 F g^{-1}[54] and 352 F g^{-1}[51] for graphene/PANI composite, 77.5% of that at 0.5 A g^{-1}. However, the specific capacitance retention is only 47.2% and 28.9% for the GOP composite and the pure PANI in the same current density range from 0.5 A g^{-1} to 20 A g^{-1}, respectively. These characteristics imply the GP composite has an excellent rate capability.

The performance of cycling stability is more crucial to the PANI-based electrode material for supercapacitors. Therefore, the cyclic performance of the GP composite was tested and compared with those of the GOP composite and the pure PANI at a scan rate of 100 mV s^{-1}, as shown in Fig. 10. For the GP composite, there is only 12.39% decay in the specific capacitance after consecutive 3000 cycles. But for the GOP composite and the pure PANI, after 2000 cycles, the specific capacitances are only retained 81.06% and 69.1%, respectively. The enhanced cycling stability is mainly because of the PANI nanowires dispersed on the surface of RGO and the intimate interaction between them. RGO sheets might effectively transfer the charges produced by faradic reaction of the PANI, which prevents PANI from severely swelling and shrinking, effectively relieves the destruction of the electrode material and leads to an outstanding stability.

Based on the above electrochemical analyses, the improved electrochemical performances of the GP composite originate from the PANI, RGO and the synergistic effect between them, as follows. (1) The PANI nanowires that are dispersed on the surface of the RGO sheets offer a relatively large contact area between the GP composite electrode and electrolyte,[17] enhancing the utilization of PANI and reducing the diffusion path and diffusion resistance of electrolyte ions into the electrode matrix. (2) The RGO serves as a substrate and intimately interacts with the PANI nanowires, which prevent the accumulation of charges produced by the faradic reaction of PANI and thereby slow down the damage in the structural conformation of the GP composite electrode during the charge and discharge process.

CONCLUSION

In summary, a facile one-pot synthesis strategy for the preparation of the GP composite has been developed based on 4-methylaniline with GO as precursor. 4-methylaniline can efficiently convert the GO into the RGO, and also act as a spacer for the resulting RGO sheets. In the GP composite, RGO sheets covered by PANI nanowires remain well-dispersed. The novel construction, which possesses a larger interfacial area, shorter ion-diffusion pathways and faster ion transport, make full use of the active materials. Therefore, this unique structure make GP composite exhibit a high specific capacitance, excellent rate capability and cycling stability compared with the GOP composite and the pure PANI. The specific capacitances are as high as 530.4 F g^{-1} and 411.1 F g^{-1} at 0.5 A g^{-1} and 20 A g^{-1}, respectively. But at the same current density, the specific capacitances for the GOP composite are respectively 440.9 F g^{-1} and 208 F g^{-1}, for the pure PANI, are respectively 367.9 F g^{-1} and 106.2 F g^{-1}. Moreover, the specific capacitance retention of the GP composite is 87.61% after 3000 cycles at 100 mV s^{-1}. It is believed that the GP composite will have a great potential for application in supercapacitors.

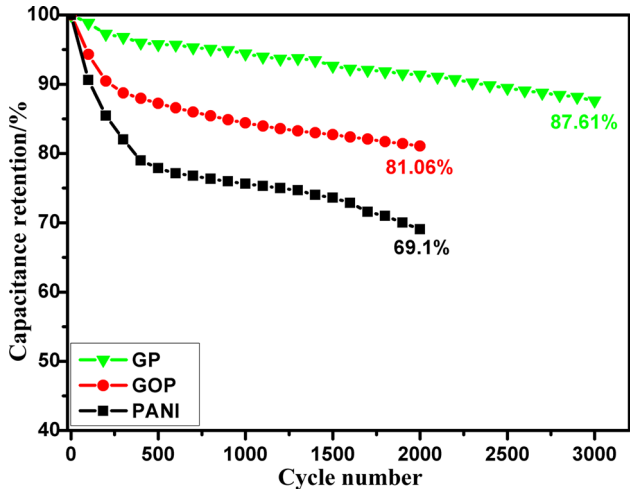

Fig. 10. Cycle stability of PANI, GOP and GP composites during the long cyclic voltammetric scans process at a scan rate of 100 mV s^{-1}.

ACKNOWLEDGMENTS

This work was supported by the National Natural Science Foundation (21664009, 51063003).

REFERENCES

1. S. Maiti and B.B. Khatua, *RSC Adv.* 3, 12874 (2013).
2. G.A. Snook, P. Kao, and A.S. Best, *J. Power Sources* 196, 1 (2011).
3. F. Rezae, N.P. Tavandashti, and A.R. Zahedi, *Res. Chem. Intermed.* 40, 1233 (2014).
4. L. Shao, Q. Wang, Z. Ma, Z. Ji, X. Wang, D. Song, Y. Liu, and N. Wang, *J. Power Sources* 379, 350 (2018).
5. H.W. Park, T. Kim, J. Huh, M. Kang, J.E. Lee, and H. Yoon, *ACS Nano* 6, 7624 (2012).
6. L. Ren, G. Zhang, J. Wang, L. Kang, Z. Lei, Z. Liu, Z. Liu, Z. Hao, and Z. Liu, *Electrochim. Acta* 145, 99 (2014).
7. B. Mu, L. Peng, and A. Wang, *Electrochim. Acta* 88, 177 (2013).
8. V. Gupta and N. Miura, *Electrochim. Acta* 52, 1721 (2006).
9. M. Baibarac, I. Baltog, C. Godon, S. Lefrant, and O. Chauvet, *Carbon* 42, 3143 (2004).

10. W. Zhao, M. Zhang, P. Pan, D. Song, S. Huang, J. Wei, X. Li, W. Qi, K. Zhanga, J. Zhao, and Z. Yang, *Surf. Coat. Technol.* 320, 595 (2017).
11. S. Guo, H. Shen, Z. Tie, S. Zhu, P. Shi, J. Fan, Q. Xu, and Y. Min, *J. Power Sources* 359, 285 (2017).
12. H. Wang, J. Liu, Z. Chen, S. Chen, T.C. Sum, J. Lin, and Z. Shen, *Electrochim. Acta* 230, 236 (2017).
13. T. Kuila, A.K. Mishra, P. Khanra, N.H. Kim, and J.H. Lee, *Nanoscale* 5, 52 (2012).
14. J. Yan, W. Tong, Z. Fan, W. Qian, M. Zhang, X. Shen, and W. Fei, *J. Power Sources* 195, 3041 (2010).
15. A. Esfandiar, O. Akhavan, and A. Irajizad, *J. Mater. Chem.* 21, 10907 (2011).
16. K. Zhang, L.L. Zhang, X.S. Zhao, and J. Wu, *Chem. Mater.* 22, 1392 (2010).
17. J. Wang, H. Xian, T. Peng, H. Sun, and F. Zheng, *RSC Adv.* 5, 13607 (2015).
18. Y. Xu, Y. Tao, X. Zheng, H. Ma, J. Luo, F. Kang, and Q.H. Yang, *Adv. Mater.* 27, 8082 (2015).
19. M. Hasan, M.M. Hossain, and M. Lee, *J. Ind. Eng. Chem.* 32, 123 (2015).
20. X. Cai, Q. Zhang, S. Wang, J. Peng, Y. Zhang, H. Ma, J. Li, and M. Zha, *J. Mater. Sci.* 49, 5667 (2014).
21. W. Zhao, D.W. He, Y.S. Wang, Y. Hu, X. Du, and X. Hao, *RSC Adv.* 5, 98241 (2015).
22. Y. Jin, M. Fang, and M. Jia, *Appl. Surf. Sci.* 308, 333 (2014).
23. N. Chen, Y. Ren, P. Kong, L. Tan, H. Feng, and Y. Luo, *Appl. Surf. Sci.* 392, 71 (2017).
24. H. Feng, B. Wang, T. Lin, N. Chen, N. Wang, and B. Chen, *J. Power Sources* 246, 621 (2014).
25. N. Chen, F. Zhang, Y. Ren, L. Tan, H. Feng, and Y. Luo, *Polym. Compos.* 40, E877 (2019).
26. W. Wu, Y. Li, L. Yang, Y. Ma, D. Pan, and Y. Li, *Electrochim. Acta* 139, 117 (2014).
27. G.M. Neelgund, A. Oki, and Z. Luo, *Mater. Res. Bull.* 48, 175 (2013).
28. Q. Wang, S. Qiu, S. Wang, J. Shang, R. Zhao, X. Wu, W. Chen, H. Zhou, and X. Wang, *Synth. Met.* 210, 314 (2015).
29. Z. Luo, L. Zhu, Y. Huang, and H. Tang, *Synth. Met.* 175, 88 (2013).
30. Y. Li, X. Zhao, Q. Xu, Q. Zhang, and D. Chen, *Langmuir* 27, 6458 (2011).
31. J. Xu, K. Wang, S.Z. Zu, B.H. Han, and Z. Wei, *ACS Nano* 4, 5019 (2010).
32. H. Sun, P. She, K.L. Xu, Y.X. Shang, S.Y. Yin, and Z.N. Liu, *Synth. Met.* 209, 68 (2015).
33. Y.F. Huang and C.W. Lin, *Polymer* 53, 2574 (2012).
34. Z. Gao, W. Yang, J. Wang, B. Wang, Z. Li, Q. Liu, M. Zhang, and L. Liu, *Energy Fuels* 27, 568 (2013).
35. Y. Yang and M. Wan, *J. Mater. Chem.* 12, 897 (2002).
36. Y. Liao, D.G. Yu, X. Wang, W. Chain, X.G. Li, E.M. Hoek, and R.B. Kaner, *Nanoscale* 5, 3856 (2013).
37. S. Xiong, Q. Wang, and Y. Chen, *Mater. Lett.* 61, 2965 (2007).
38. Y. Feng, N. Feng, and G. Du, *RSC Adv.* 3, 21466 (2013).
39. A.C. Ferrari and J. Robertson, *Phys. Rev. B Condens. Matter* 61, 14095 (2000).
40. M.S. Ramasamy, S.S. Mahapatra, D.H. Yi, H.J. Yoo, and J.W. Cho, *RSC Adv.* 4, 23936 (2014).
41. H.P. Cong, X.C. Ren, P. Wang, and S.H. Yu, *Energ Environ. Sci.* 6, 11851 (2013).
42. J. Luo, L.J. Cote, V.C. Tung, A.T.L. Tan, P.E. Goins, J. Wu, and J. Huang, *J. Am. Chem. Soc.* 132, 17667 (2010).
43. P. Gong, Z. Wang, Z. Fan, W. Hong, Z. Yang, J. Wang, and S. Yang, *Carbon* 72, 176 (2014).
44. V.H. Nguyen, L. Tang, and J.J. Shim, *Colloid Polym. Sci.* 291, 2237 (2013).
45. X.M. Feng, R.M. Li, Y.W. Ma, R.F. Chen, N.E. Shi, Q.L. Fan, and W. Huang, *Adv. Funct. Mater.* 21, 2989 (2011).
46. L. Chen, J. Lei, F. Wang, G. Wang, and H. Feng, *RSC Adv.* 5, 40148 (2015).
47. S. Chen, J. Zhu, X. Wu, Q. Han, and X. Wang, *ACS Nano* 4, 2822 (2010).
48. X. Li, Q. Zhong, X. Zhang, T. Li, and J. Huang, *Thin Solid Films* 584, 348 (2015).
49. F. Yang, M. Xu, S.J. Bao, H. Wei, and H. Chai, *Electrochim. Acta* 137, 381 (2014).
50. J. Luo, Q. Ma, H. Gu, Y. Zheng, and X. Liu, *Electrochim. Acta* 173, 184 (2015).
51. Y. Yang, Y. Xi, J. Li, G. Wei, N.I. Klyui, and W. Han, *Nanoscale Res. Lett.* 12, 394 (2017).
52. J. Chen, J. Song, and X. Feng, *Polym. Bull.* 74, 27 (2017).
53. R.I. Jafri Jaidev, A.K. Mishra, and S. Ramaprabhu, *J. Mater. Chem.* 2, 17601 (2011).
54. J. Luo, W. Zhong, Y. Zou, C. Xiong, and W. Yang, *J. Power Sources* 319, 73 (2016).